

# Discovery of a Jupiter/Saturn Analog with Gravitational Microlensing

B.S. Gaudi<sup>1,\*</sup>, D.P. Bennett<sup>2</sup>, A. Udalski<sup>3</sup>, A. Gould<sup>1</sup>,  
G.W. Christie<sup>4</sup>, D. Maoz<sup>5</sup>, S. Dong<sup>1</sup>, J. McCormick<sup>6</sup>,  
M.K. Szymański<sup>3</sup>, P.J. Tristram<sup>7</sup>, S. Nikolaev<sup>8</sup>,  
B. Paczyński<sup>9,†</sup>, M. Kubiak<sup>3</sup>, G. Pietrzyński<sup>3,10</sup>, I. Soszyński<sup>3</sup>,  
O. Szewczyk<sup>3</sup>, K. Ulaczyk<sup>3</sup>, Ł. Wyrzykowski<sup>3,11</sup>

(The OGLE Collaboration)

D.L. DePoy<sup>1</sup>, C. Han<sup>12</sup>, S. Kaspi<sup>5</sup>, C.-U. Lee<sup>13</sup>, F. Mallia<sup>14</sup>,  
T. Natusch<sup>4</sup>, R.W. Pogge<sup>1</sup>, B.-G. Park<sup>13</sup>, (The  $\mu$ FUN Collaboration)  
F. Abe<sup>15</sup>, I.A. Bond<sup>16</sup>, C.S. Botzler<sup>17</sup>, A. Fukui<sup>15</sup>, J.B. Hearnshaw<sup>18</sup>,  
Y. Itow<sup>15</sup>, K. Kamiya<sup>15</sup>, A.V. Korpela<sup>19</sup>, P.M. Kilmartin<sup>7</sup>, W. Lin<sup>16</sup>,  
K. Masuda<sup>15</sup>, Y. Matsubara<sup>15</sup>, M. Motomura<sup>15</sup>, Y. Muraki<sup>20</sup>, S. Nakamura<sup>15</sup>,  
T. Okumura<sup>15</sup>, K. Ohnishi<sup>21</sup>, N.J. Rattenbury<sup>22</sup>, T. Sako<sup>15</sup>, To. Saito<sup>23</sup>,  
S. Sato<sup>24</sup>, L. Skuljan<sup>16</sup>, D.J. Sullivan<sup>19</sup>, T. Sumi<sup>15</sup>, W.L. Sweatman<sup>16</sup>,  
P.C.M. Yock<sup>17</sup>, (The MOA Collaboration)

M.D. Albrow<sup>18</sup>, A. Allan<sup>25</sup>, J.-P. Beaulieu<sup>26</sup>, M.J. Burgdorf<sup>27</sup>, K.H. Cook<sup>8</sup>,  
C. Coutures<sup>26</sup>, M. Dominik<sup>28,‡</sup>, S. Dieters<sup>29</sup>, P. Fouqué<sup>30</sup>, J. Greenhill<sup>29</sup>,  
K. Horne<sup>28</sup>, I. Steele<sup>27</sup>, Y. Tsapras<sup>27</sup>,

(From the PLANET and RoboNet Collaborations)

B. Chaboyer<sup>31</sup>, A. Crocker<sup>32</sup>, S. Frank<sup>1</sup>, B. Macintosh<sup>8</sup>

October 28, 2018

<sup>1</sup>Department of Astronomy, Ohio State University, 140 West 18th Avenue, Columbus, OH 43210, USA

\*To whom correspondence should be addressed; E-mail: [gaudi@astronomy.ohio-state.edu](mailto:gaudi@astronomy.ohio-state.edu)

<sup>2</sup>Department of Physics, 225 Nieuwland Science Hall, Notre Dame University, Notre Dame, IN 46556, USA

<sup>3</sup>Warsaw University Observatory, Al. Ujazdowskie 4, 00-478 Warszawa, Poland

- <sup>4</sup>Auckland Observatory, P.O. Box 24-180, Auckland, New Zealand
- <sup>5</sup>School of Physics and Astronomy, Raymond and Beverley Sackler Faculty of Exact Sciences, Tel-Aviv University, Tel Aviv 69978, Israel
- <sup>6</sup>Farm Cove Observatory, 2/24 Rapallo Place, Pakuranga, Auckland 1706, New Zealand
- <sup>7</sup>Mt. John Observatory, P.O. Box 56, Lake Tekapo 8770, New Zealand
- <sup>8</sup>IGPP, Lawrence Livermore National Laboratory, 7000 East Ave., Livermore, CA 94550, USA
- <sup>9</sup>Princeton University Observatory, Princeton, NJ 08544, USA
- <sup>†</sup>Deceased
- <sup>10</sup>Universidad de Concepción, Departamento de Física, Casilla 160–C, Concepción, Chile
- <sup>11</sup>Institute of Astronomy, University of Cambridge, Madingley Road, Cambridge CB3 0HA, UK
- <sup>12</sup>Program of Brain Korea, Department of Physics, Chungbuk National University, 410 Seongbong-Rho, Hungduk-Gu, Chongju 371-763, Korea
- <sup>13</sup>Korea Astronomy and Space Science Institute, 61-1 Hwaam-Dong, Yuseong-Gu, Daejeon 305-348, Korea
- <sup>14</sup>Campo Catino Astronomical Observatory, P.O. Box Guarcino, Frosinone 03016, Italy
- <sup>15</sup>Solar-Terrestrial Environment Laboratory, Nagoya University, Nagoya, 464-8601, Japan
- <sup>16</sup>Institute for Information and Mathematical Sciences, Massey University, Private Bag 102-904, Auckland 1330, New Zealand
- <sup>17</sup>Department of Physics, University of Auckland, Private Bag 92-019, Auckland 1001, New Zealand
- <sup>18</sup>University of Canterbury, Department of Physics and Astronomy, Private Bag 4800, Christchurch 8020, New Zealand
- <sup>19</sup>School of Chemical and Physical Sciences, Victoria University, Wellington, New Zealand
- <sup>20</sup>Department of Physics, Konan University, Nishiokamoto 8-9-1, Kobe 658-8501, Japan
- <sup>21</sup>Nagano National College of Technology, Nagano 381-8550, Japan
- <sup>22</sup>Jodrell Bank Centre for Astrophysics, The University of Manchester, Manchester, M13 9PL, UK
- <sup>23</sup>Tokyo Metropolitan College of Aeronautics, Tokyo 116-8523, Japan
- <sup>24</sup>Department of Physics and Astrophysics, Faculty of Science, Nagoya University, Nagoya 464-8602, Japan
- <sup>25</sup>School of Physics, University of Exeter, Stocker Road, Exeter, EX4 4QL, UK
- <sup>26</sup>Institut d’Astrophysique de Paris, CNRS, Universit Pierre et Marie Curie UMR7095, 98bis Boulevard Arago, 75014 Paris, France
- <sup>27</sup>Astrophysics Research Institute, Liverpool John Moores University, Twelve Quays House, Egerton Wharf, Birkenhead CH41 1LD, UK
- <sup>28</sup>SUPA, University of St Andrews, School of Physics & Astronomy, North Haugh, St Andrews, KY16 9SS, UK
- <sup>‡</sup>Royal Society University Research Fellow
- <sup>29</sup>University of Tasmania, School of Mathematics and Physics, Private Bag 37, Hobart, TAS 7001, Australia

<sup>30</sup>Observatoire Midi-Pyrénées, Laboratoire d’Astrophysique, UMR 5572, Université Paul Sabatier–Toulouse 3, 14 avenue Edouard Belin, 31400 Toulouse, France

<sup>31</sup>Department of Physics and Astronomy, Dartmouth College, 6127 Wilder Laboratory, Hanover, NH 03755, USA

<sup>32</sup>University of Oxford, Denys Wilkinson Building, Keble Road, Oxford, OX1 3RH, UK

**Searches for extrasolar planets have uncovered an astonishing diversity of planetary systems, yet the frequency of solar system analogs remains unknown. The gravitational microlensing planet search method is potentially sensitive to multiple-planet systems containing analogs of all the solar system planets except Mercury. We report the detection of a multiple-planet system with microlensing. We identify two planets with masses of  $\sim 0.71$  and  $\sim 0.27$  times the mass of Jupiter and orbital separations of  $\sim 2.3$  and  $\sim 4.6$  astronomical units orbiting a primary star of mass  $\sim 0.50$  solar masses at a distance of  $\sim 1.5$  kiloparsecs. This system resembles a scaled version of our solar system in that the mass ratio, separation ratio, and equilibrium temperatures of the planets are similar to those of Jupiter and Saturn. These planets could not have been detected with other techniques; their discovery from only six confirmed microlensing planet detections suggests that solar system analogs may be common.**

Nearly 250 extrasolar planets (*1*) have been discovered by measuring a variety of effects: reflex motion of the host star using pulsar timing or precision Doppler measurements (*2, 3, 4*); periodic dimming of the parent star as the planet transits in front (*5, 6*); and planet-induced perturbations to microlensing light curves in which the host star acts as the primary gravitational lens (*7, 8, 9, 10, 11*). These detections have uncovered an enormous range of planetary properties, indicating that planetary systems very unlike our own are common throughout the Galaxy (*12*).

To date,  $\sim 25$  multiple-planet systems have been detected (*13*), all but one (*2*) using the Doppler method. Because Doppler surveys must monitor the host star’s reflex motion over the planet’s orbital period, they are limited by the finite duration as well as the sensitivity of the measurements. Hence, they are only just now becoming sensitive to Jupiter analogs and are not yet sensitive to Saturn analogs (nor, ipso facto, Jupiter/Saturn systems). Thus, all multiple-planet systems discovered so far are very dissimilar from our own, and the frequency of solar system analogs remains unknown.

Because microlensing relies on the direct perturbation of light from distant stars by the gravitational field of the planet, it is ‘instantaneously’ able to detect planets without requiring observations over a full orbit. For a primary star of mass  $M$ , microlensing sensitivity peaks for planets in the range  $\sim [1 - 5](M/0.3M_{\odot})^{1/2}$  astronomical units (AU) (*14*). For solar-mass stars, this is exactly the range of the solar system gas giants so microlensing provides a method to probe solar system analogs (*14, 15*).

As pointed out by Griest & Safizadeh (16), the very rare class of high-magnification ( $> 100$ ) microlensing events provides an extremely sensitive method of detecting planets. Near the peak of high-magnification events, the two images created by the primary star are highly magnified and distorted, and form a complete or nearly complete Einstein ring. A planetary companion to the primary star lying reasonably near the Einstein ring will distort the symmetry of the ring. As the host passes very close to the source line-of-sight, the images sweep around the Einstein ring, thus probing this distortion. Although the total number of high-magnification events is small, the instantaneous chance of detection in each is much higher than for the more common low-magnification events. Equally important, the interval of high-sensitivity (i.e., high-magnification) is predictable from the evolution of the light curve (16, 17, 18, 19). This permits concentration of scarce observing resources on these events. Furthermore, the high-magnification makes it possible to acquire high signal-to-noise ratio photometry of the peak of the events using relatively small-aperture (and so plentiful) telescopes. As a result, four (9, 11) of the six planets (8, 10) discovered to date in microlensing events were in high-magnification events.

Almost immediately after Griest and Safizadeh (16) pointed out the sensitivity of high-magnification events, Gaudi et al. (20) derived an important corollary. Because planets in the neighborhood of the Einstein ring are revealed with near unit probability in high-magnification events, multiple-planet systems lying in this region will be revealed with almost the same probability.

The Optical Gravitational Lens Experiment (OGLE) (21) and Microlensing Observations in Astrophysics (MOA) (19) collaborations together alert  $\sim 700$  ongoing microlensing events per year. Two collaborations, a joint venture of the Probing Lensing Anomalies NETwork (PLANET) (22) and RoboNet (23) collaborations, and the Microlensing Follow-Up Network ( $\mu$ FUN) (24), then monitor a subset of these alerts to search for planets.  $\mu$ FUN focuses almost entirely on high-magnification events, including two events originally alerted by OGLE that proved to have a Jupiter-mass (9) and a Neptune-mass (11) planet, respectively. Here, we report on the detection of a multi-planet system using this approach.

On 28 March 2006 (HJD  $\sim 3822$ ), the OGLE Early Warning System (EWS) (21) announced OGLE-2006-BLG-109 as a non-standard microlensing event possibly indicative of a planet. This immediately triggered followup observations by  $\mu$ FUN and RoboNet, which gained intensity as the event approached high-magnification. On 5 April, the event underwent a deviation from the single-lens form indicative of a binary lens. Within 12 hours of this deviation, a preliminary model indicated a jovian-class planet, which was predicted to generate an additional peak on 8 April. The 8 April peak occurred as predicted, but in the meantime, there was an additional peak on 5/6 April, which turned out to be due to a second Jovian-class planet.

Figure 1 shows the data from 11 observatories, including 7 from  $\mu$ FUN [the Auckland 0.35m and Farm Cove 0.25m in New Zealand (clear filter), the Wise 1m in Israel (clear), the CTIO/SMARTS 1.3m in Chile (*I*-band and *H*-band), the Areo8 0.3m in New Mexico operated by the Campo Catino Astronomical Observatory (clear), and the MDM 2.4m (*I*-band) and Mt. Lemmon 1.0m (*I*-band) in Arizona], the OGLE Warsaw 1.3m (*I*-band) in Chile, the MOA Mt.

John 0.6m (*I*-band) in New Zealand, the PLANET/Canopus 1m (*I*-band) in Tasmania, and the RoboNet/Liverpool 2m (*R*-band) in the Canary Islands. There are a total of 2642 data points. In addition, there are 29 V-band data points from OGLE and CTIO/SMARTS that we use to determine the source color.

The qualitative character of the event can be read directly from the light curve, primarily from the five distinctive features shown in Figure 2. Consider the first three features: the low-amplitude anomaly (OGLE, HJD $\sim$  3823) that triggered the OGLE EWS alert, the gentle “shoulder” during the first rise (MOA, HJD $\sim$  3830), and the first peak (Auckland, HJD $\sim$  3831). Together, these can only be produced by, respectively, passage close to or over a weak cusp, entrance into a weak caustic, and exit from a strong caustic. (The magnification diverges when a point source crosses a closed concave caustic curve, where additional images are created on entry or destroyed on exit of the enclosed area. Caustics are strong or weak depending on the brightness of these images. The concave curves meet at cusps that produce sharp spikes of magnification when crossed by the source.) Such a sequence requires a topology similar to the one shown in the inset to Figure 1. The specific strengths of each feature require the specific caustic topology shown. In particular, the narrow mouth of the caustic toward the bottom generates a very strong caustic. This was essentially the argument used to predict the fifth feature (OGLE/MDM/Lemmon/Auckland/FarmCove/Tasmania, HJD $\sim$  3834), corresponding to a moderately strong cusp passage (Fig. 1). The size and strength of this caustic imply a jovian-class planet lying very close to the Einstein ring, although detailed modeling is required to derive the precise planet/star mass ratio. The fourth feature (Wise/OGLE, HJD $\sim$  3831.5) cannot be explained by considering the caustic generated by this jovian-class planet alone. This feature occurs near the time when the source approaches closest to the center-of-mass of the planet/star system; this is exactly the time at which the central-caustic bumps due to additional planets are expected to occur (20). The inset in Figure 1 highlights the additional caustic feature due to a second planet that is required to explain this bump. This caustic feature is smaller than the main caustic, which implies that the planet, also of jovian class, lies farther from the Einstein ring, so it is subject to the standard (16)  $b \leftrightarrow b^{-1}$  degeneracy, where  $b$  is the planet-star projected separation in units of the Einstein radius. A detailed analysis shows the mass is three times as great as that of the first planet and that the  $b < 1$  solution is favored by  $\Delta\chi^2 = 11.4$ . We label these planets OGLE-2006-BLG-109Lc and OGLE-2006-BLG-109Lb, respectively. Although the caustics of the individual planets do interact to form a single caustic curve, their effects are nevertheless mostly independent (25, 18, 26), so the parts of the caustic associated with the individual planets can be identified, as shown in Figure 1. Modeling the light curve in detail with a three-body lens yields,  $m_b/M = 1.35 \times 10^{-3}$ ,  $m_c/m_b = 0.36$  for the mass ratio of the planets and their host, very similar to  $m_j/M_\odot = 0.96 \times 10^{-3}$  and  $m_s/m_j = 0.30$  for Jupiter, Saturn, and the Sun. The ratio of projected separations  $r_{\perp,b}/r_{\perp,c} = 0.60$  is also very similar to the Jupiter/Saturn value of  $a_j/a_s = 0.55$ .

Two subgroups of authors conducted independent searches for alternative solutions. Both found that no single-planet solution is consistent with the light-curve topology. We also successively eliminated each of the five features to see whether the remaining four features could be fit

by a single planet. We found that only the elimination of the fourth feature produced successful single-planet models. By contrast, similar procedures in other events (11, 27) led to many independent solutions. OGLE-2006-BLG-109 differs from these in that it has five well-covered features.

Several higher-order effects are apparent in this event that permit us to extract much more detailed information about the system from the light curve. We only briefly sketch these here. For over 95% of microlensing events observed from the ground, the lens parameters are determined only relative to the angular Einstein radius  $\theta_E$ , whose absolute scale remains unknown. Here  $\theta_E = \sqrt{4GM/c^2 D}$ , where  $M$  is the mass of the lens,  $1/D \equiv 1/D_l - 1/D_s$ , and  $D_l$  and  $D_s$  are the distances to the lens and the source, respectively. However, in this event the effect of the finite size of the source star during caustic exit allows us to measure the source radius relative to the Einstein radius,  $\rho = \theta_*/\theta_E$  (28). From the source color and flux we can determine its angular size  $\theta_*$ , and thus  $\theta_E$  (24).

The acceleration of Earth in its orbit about the Sun induces subtle distortions on the light curve called microlens parallax, which yields the physical size of the Einstein radius projected onto the observer plane,  $\tilde{r}_E \equiv \theta_E D$  (29). This is usually measured only in the roughly 3% of events that are extremely long, but this event happens to be long and so displays clear distortions arising from parallax.

Combining these two measures of the Einstein radius allows us to triangulate the event and so determine the host star distance,  $D_l = 1/(\theta_E/\tilde{r}_E + 1/D_s)$ , and mass,  $M = (c^2/4G)\tilde{r}_E\theta_E$ . We assume  $D_s = 8$  kpc, although our results are insensitive to this assumption. From a preliminary analysis we infer  $D_l \simeq 1.5$  kpc and  $M \simeq 0.5 M_\odot$ . Based on high-resolution Keck AO  $H$ -band images, we detect light from the lens and infer its magnitude to be  $H = 17.17 \pm 0.25$ , consistent with the mass estimate from the light curve. We subsequently incorporate the lens flux constraint in the light curve analysis, which allows us to derive more precise estimates of  $D_l = 1.49 \pm 0.13$  kpc and  $M = 0.50 \pm 0.05 M_\odot$ . The planet masses are  $m_b = 0.71 \pm 0.08$  and  $m_c = 0.27 \pm 0.03$  times the mass of Jupiter.

Finally, we also detect the orbital motion of the outer planet; this motion both rotates and changes the shape of the larger caustic shown in the top inset to Figure 1. We are able to constrain the two components of the projected velocity of the planet relative to the primary star. Together with the estimate of the stellar mass, they completely determine the outer planet's orbit (including inclination) under the assumption that it is circular, up to a two-fold degeneracy. The solution presented here is marginally favored by the data at  $\Delta\chi^2 = 4.8$  via the effect of the planet's acceleration on the light curve. Thus we can estimate the full (three-dimensional) separation of planet c (again assuming a circular orbit), and also of planet b (assuming a coplanar and circular orbit). We find  $a_b = 2.3 \pm 0.2$  AU and  $a_c = 4.6 \pm 0.5$  AU. A more refined estimate of these parameters and their uncertainties will require a detailed analysis including the combined effects of finite sources, parallax, and orbital motion of the planets. The results of this analysis will be presented elsewhere (Bennett et al., in preparation).

The OGLE-2006-BLG-109L planetary system bears a remarkable similarity to our own solar system. Although the primary mass is only half solar, the mass ratio of the two planets

(0.37) and separation ratio (0.50) are similar to those of Jupiter and Saturn. We infer their equilibrium temperatures to be  $T_{\text{eq}} \sim 82 \pm 12$  K and  $T_{\text{eq}} \sim 59 \pm 7$  K,  $\sim 30\%$  smaller than those of Jupiter and Saturn.

Before the detection of extrasolar planets, planet formation theories generally predicted that other systems should resemble our solar system. In the core-accretion paradigm, the most massive giant planet forms at the ‘snow line,’ the point in the protoplanetary disk exterior to which ices are stable. Immediately beyond the snow line, the surface density of solids is highest and the dynamical time is the shortest, and therefore the timescale for planet formation is the shortest. Beyond the snow line, the formation timescale increases with distance from the host star. Thus in this ‘classical’ picture of planet formation, one would expect planet mass to decrease with increasing distance beyond the snow line, as is observed in our solar system (30). The discovery of a population of massive planets well interior to the snow line demonstrated that this picture of planet formation is incomplete, and considerable inward migration of planets must occur (31). Nevertheless, this classical picture may still be applicable to our solar system and some fraction of other systems as well. The OGLE-2006-BLG-109L planetary system represents just such a ‘scaled version’ of our own solar system, with a less-massive host. This system preserves the mass-distance correlation in our solar system, and the scaling with primary mass is consistent with the core-accretion paradigm in which giant planets that form around lower-mass stars are expected to be less massive but form in regions of the protoplanetary disk with similar equilibrium temperatures and are therefore closer to their parent star (32).

The majority of the  $\sim 25$  known multi-planet systems are quite dissimilar to the OGLE-2006-BLG-109L system and to our own solar system. Many of these systems have the very close-in massive planets indicative of large-scale planetary migration, or they have a ‘normal hierarchy’, in which the masses of the giant planets increase with distance from the parent star. There are two multi-planet systems with properties roughly similar to those of OGLE-2006-BLG-109L. The 47 UMa and 14 Her systems each contain a giant planet at a semimajor axis of  $\sim 3$  AU and a second, less massive giant planet at a separation of  $\sim 7$  AU (33). However, because of their higher-mass primaries, the equilibrium temperatures of these planets are considerably higher than those of OGLE-2006-BLG-109L or Jupiter and Saturn, so these systems cannot be considered close analogs of our solar system.

OGLE-2006-BLG-109Lb and OGLE-2006-BLG-109Lc are the fifth and sixth planets to be detected by microlensing. Although, given the detection of planet c, the *a priori* probability of detecting planet b in this event was high, it was not unity. Furthermore, only two other jovian-mass planets have been detected by microlensing (8, 9), and neither event had substantial sensitivity to multiple planets. These facts may indicate that the stars being probed by microlensing that host jovian-mass companions are also likely to host additional giant planets. If the OGLE-2006-BLG-109L planetary system is typical, these systems may have properties similar to our solar system. Regardless, the detection of the OGLE-2006-BLG-109L planetary system demonstrates that microlensing surveys will be able to constrain the frequency of solar system analogs throughout the Galaxy.

## References and Notes

1. J. Schneider (2006); <http://exoplanet.eu>
2. A. Wolszczan, D. A. Frail, *Nature* **355**, 145 (1992).
3. M. Mayor, M., D. Queloz, D. *Nature* **378**, 355 (1995).
4. G. W. Marcy, & R. P. Butler, *Astrophys. J.* **464**, L147 (1996).
5. A. Udalski, et al. *Acta Astron.* **52**, 1 (2002).
6. M. Konacki, et al. *Nature* **421**, 507 (2003).
7. S. Mao & B. Paczyński, *Astrophys. J.* **374**, L37 (1991).
8. I. A. Bond, et al., *Astrophys. J.* **606**, L155 (2004).
9. A. Udalski, et al. *Astrophys. J.* **628**, L109 (2005).
10. J.-P. Beaulieu et al., *Nature* **439**, 437 (2006).
11. A. Gould, et al. *Astrophys. J.* **644**, L37 (2006).
12. D. A. Fischer, J. Valenti, *Astrophys. J.* **622**, 1102 (2005).
13. R. P. Butler, et al., *Astrophys. J.* **646**, 505 (2006).
14. A. Gould, A. Loeb, *Astrophys. J.* **396**, 104 (1992).
15. D. P. Bennett, S. H. Rhie, *Astrophys. J.* **574**, 985 (2002).
16. K. Griest, N. Safizadeh, *Astrophys. J.* **500**, 37 (1998).
17. S. H. Rhie, et al., *Astrophys. J.* **533**, 378 (2000).
18. N. J. Rattenbury, I. A. Bond, J. Skuljan, P. C. M. Yock, *Mon. Not. R. Astron. Soc.* **335**, 159 (2002).
19. F. Abe, F., et al., *Science* **305**, 1264 (2004)
20. B. S. Gaudi, R. M. Naber, P. D. Sackett, *Astrophys. J.* **502**, L33 (1998).
21. A. Udalski, *Acta Astron.* **53**, 291 (2003).
22. M.D. Albrow, *Astrophys. J.* **509**, 687 (1998).
23. M. J. Burgdorf, et al., *Planetary and Space Science* **55**, 582 (2007)



24. J. Yoo, et al., *Astrophys. J.* **603**, 139 (2004).
25. J. Wambsganss, *Mon. Not. R. Astron. Soc.* **284**, 172 (1997)
26. C. Han, *Astrophys. J.* **629**, 1102 (2005)
27. S. Dong, et al., *Astrophys. J.* **664**, 862 (2007)
28. A. Gould, *Astrophys. J.* **421**, L71 (1994).
29. A. Gould, *Astrophys. J.* **392**, 442 (1992).
30. J. J. Lissauer, *Icarus* **69**, 249 (1987).
31. D. N. C. Lin, P. Bodenheimer, D. C. Richardson, *Nature* **380**, 606 (1996)
32. S. Ida, & D. N. C. Lin, *Astrophys. J.* **626**, 1045 (2005)
33. R. A. Wittenmyer, R. A., *Astrophys. J.* **654**, 625 (2007)
34. We acknowledge the following support: NSF AST-042758 (AG,SD); NASA NNG04GL51G (DD,AG,RP); NASA/JPL 1226901 (DD,BSG,AG); Polish MNiSW N20303032/4275 (OGLE); NSF AST-0708890, NASA NNX07AL71G (DPB); SRC Korea Science & Engineering Foundation (CH); Korea Astronomy & Space Science Institute (B-GP); Deutsche Forschungsgemeinschaft (CSB); PPARC, EU FP6 programme “ANGLES” (ŁW,SM,NJR); PPARC (RoboNet); Israel Science Foundation (DM); Marsden Fund of NZ, Japan Ministry of Education, Culture, Sports, Science and Technology, Japan Society for the Promotion of Science (MOA) RoboNet-1.0 is funded by STFC and operates in conjunction with the eSTAR project, which supports AA, and which is jointly funded by the DTI, STFC and EPSRC. KHC’s, SN’s and BM’s work performed under the auspices of the U.S. Department of Energy by Lawrence Livermore National Laboratory under Contract DE-AC52-07NA27344. We thank the MDM staff for their support. We thank David Warren for financial support for the Mt. Canopus Observatory. We thank Mike Bode, Dan Bramich, Chris Mottram, Steve Fraser, and Colin Snodgrass for contributions to the RoboNet data.

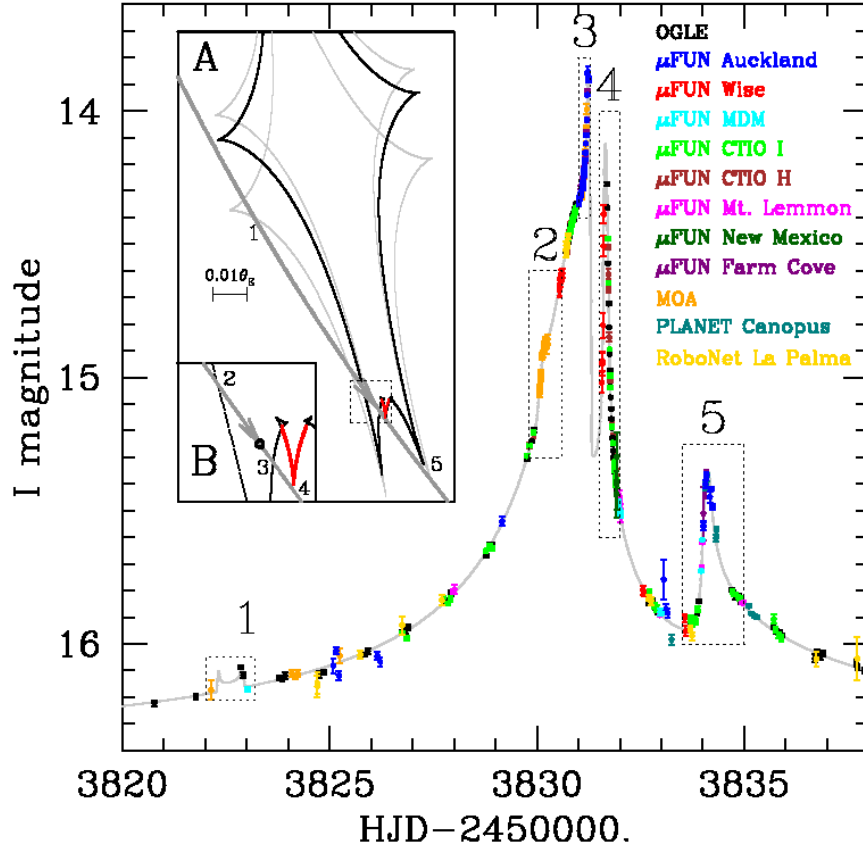


Figure 1: Data and best-fit model of the OGLE-2006-BLG-109Lb,c two-planet system. The data have been binned for clarity, although the fitting procedures used the unbinned data. Data from each different observatory/filter combination (as indicated by the color scheme) have been aligned using a linear fit to the magnification, which introduces negligible uncertainties. Only data near the peak of the event are shown (the unlensed magnitude is  $I = 16.42$ ). Panel A: The source trajectory through the caustic created by the two-planet system is shown as the dark grey curve with the arrow indicating the direction of motion. The horizontal line shows an angular scale of  $0.01 \theta_E$ , or  $\sim 15 \mu\text{as}$ . The shape and orientation of the caustic due to both planets at the peak of the event is shown by the black curve. The five light-curve features detailed in Fig. 2 are caused by the source crossing or approaching the caustic; the approximate locations of the features are labeled with numbers. The majority of the caustic (in black) is due to only the outer (Saturn-analog) planet; this portion of the caustic explains four of the five features. The portion arising from the second (Jupiter-analog) planet is highlighted in red. This additional cusp in the caustic is required to explain the fourth feature in the light curve; as such, the fourth feature signals the presence of a second (Jupiter-analog) planet. Because of the orbital motion of the Saturn-analog planet, the shape and orientation of the caustic changes over the course of the event. The light grey curves show the caustic at the time of features 1 and 5. Panel B: A zoom of the source trajectory and caustic near the times of the second, third, and fourth features. The circle shows the size of the source.

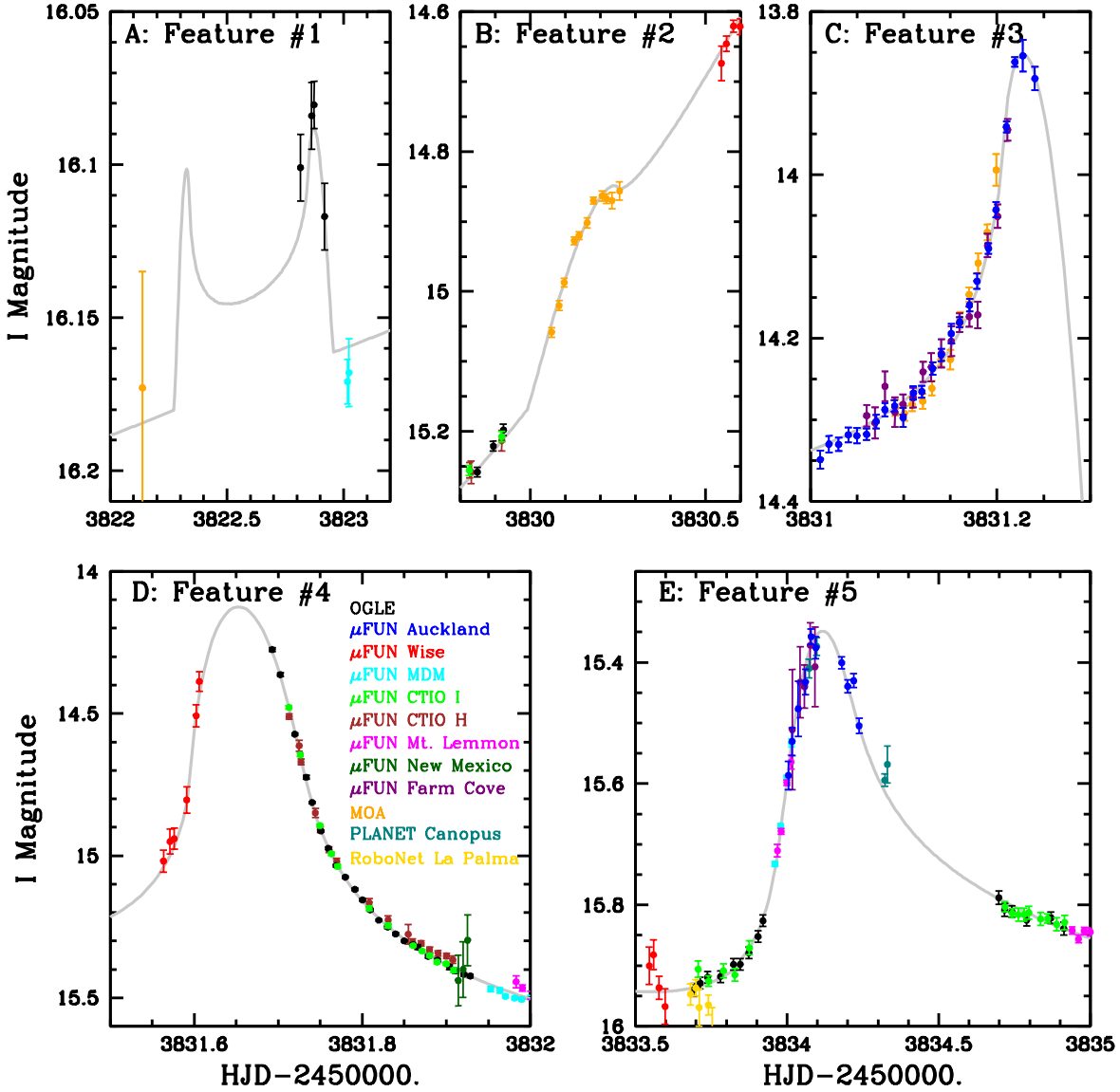


Figure 2: Five features of light curve from Fig. 1, which determine planetary geometry. A) Feature 1: weak cusp crossing; B) Feature 2: weak caustic entrance; C) Feature 3: strong caustic exit; D) Feature 4: strong cusp approach; E) Feature 5: moderate cusp approach. Features 1, 2, 3, and 5, are explained by the black portion of the caustic seen in in Fig. 1A. Feature 4 requires an additional cusp in the caustic, which is shown as the red curve. Data have been binned for clarity.